INTERNATIONAL JOURNAL FOR NUMERICAL METHODS IN FLUIDS, VOL. 10, 285–303 (1990)

CASCADE AERODYNAMIC GUST RESPONSE INCLUDING STEADY LOADING EFFECTS

HSIAO-WEI D. CHIANG AND SANFORD FLEETER

Thermal Sciences and Propulsion Center, School of Mechanical Engineering, Purdue University, West Lafayette, IN 47907, U.S.A.

SUMMARY

To predict the unsteady convected gust aerodynamic response of a cascade comprised of arbitrary thick and cambered aerofoils in an incompressible, inviscid, flow field, a complete first-order model is formulated. The flow is analysed by considering a periodic flow channel. The velocity potential is separated into steady and unsteady harmonic components, each described by a Laplace equation. The strong dependence of the unsteady aerodynamics on the steady effects of aerofoil and cascade geometry and incidence angle is manifested in the coupling of the unsteady and steady flow fields through the unsteady boundary conditions. Analytical solutions in individual grid elements of a body-fitted computational grid are then determined, with the complete solution obtained by assembly of these local solutions. The validity and capabilities of this model and solution technique are then demonstrated by analysing the steady and unsteady aerodynamics of both theoretical and experimental cascade configurations.

INTRODUCTION

Unsteady aerodynamic gust models have typically been restricted to thin aerofoil theory, with the unsteady gust-generated flow field assumed to be small as compared to the steady mean potential flow. In addition, the aerofoils are considered to be flat plates at zero incidence. Thus the unsteady aerodynamics uncouples from the steady flow, resulting in models wherein the flow is linearized about a uniform parallel flow. Such models have considered convected gusts, including transverse gusts for both isolated aerofoils and cascades[1,2] and linearly combined transverse and chordwise gusts for isolated aerofoils.[3,4] Unfortunately, these linearized models are only approximate, having neglected second-order terms. Thus they cannot be extended to finite incidence angles or realistic cambered profiles, i.e. loaded aerofoils and cascades.

In many applications, e.g. fluid machinery, cascades comprised of aerofoils with large camber and thickness which operate at finite incidence angle to a non-parallel mean flow field are required. Unfortunately, the classical thin aerofoil approach is not adequate for such applications. For an isolated aerofoil, Goldstein and Atassi[5] and Atassi[6] developed a theory for the inviscid incompressible flow past the single aerofoil subject to an interacting periodic gust. The theory assumes that the fluctuating flow velocity is small compared to the mean velocity, with the unsteady flow linearized about the full potential steady flow past the aerofoil, which accounts for the effects of aerofoil geometry and mean flow angle of attack.

In this paper the convected gust-generated unsteady aerodynamic response of an arbitrary aerofoil cascade in an incompressible, inviscid, flow field is analysed. This is accomplished by

0271–2091/90/030285–19$09.50 *Received August 1988*
© 1990 by John Wiley & Sons, Ltd.

formulating and developing a complete first-order model, i.e. the classical thin aerofoil theory assumption of the steady flow being uniform and parallel is not used, to predict the incompressible, unsteady aerodynamics generated by a two-dimensional gust convected with the steady mean flow past an arbitrary cascade comprised of thick, cambered aerofoils at non-zero mean flow incidence angle. The unsteady flow field is considered to be rotational and is linearized about the full steady potential flow past the cascade. Thus the effects of aerofoil profile and mean flow incidence are completely accounted for through the mean potential flow field. The steady potential flow field and the potential component of the unsteady flow are individually described by Laplace equations, with the unsteady potential decomposed into circulatory and non-circulatory parts. The steady potential is independent of the unsteady flow. However, the strong dependence of the unsteady aerodynamics on the steady effects of aerofoil and cascade geometry and incidence angle are manifested in the coupling of the unsteady and steady flow fields through the unsteady boundary conditions.

A locally analytical solution is developed. In this technique the discrete algebraic equations which represent the flow field equations are obtained from analytical solutions in individual grid elements. A body-fitted computational grid is utilized. General analytical solutions to the transformed Laplace equations are developed by applying these solutions to individual grid elements, i.e. the integration and separation constants are determined from the boundary conditions in each grid element. The complete flow field is then determined by assembling these locally analytical solutions.

MATHEMATICAL MODEL

Figure 1 presents a schematic representation of a thick, cambered aerofoil cascade at finite mean flow incidence α_0 to the far-field uniform mean flow $\mathbf{U}_\infty = U_\infty \mathbf{i}$, with a superimposed convected two-dimensional harmonic gust. The cascade has a stagger angle of δ, with S the distance between

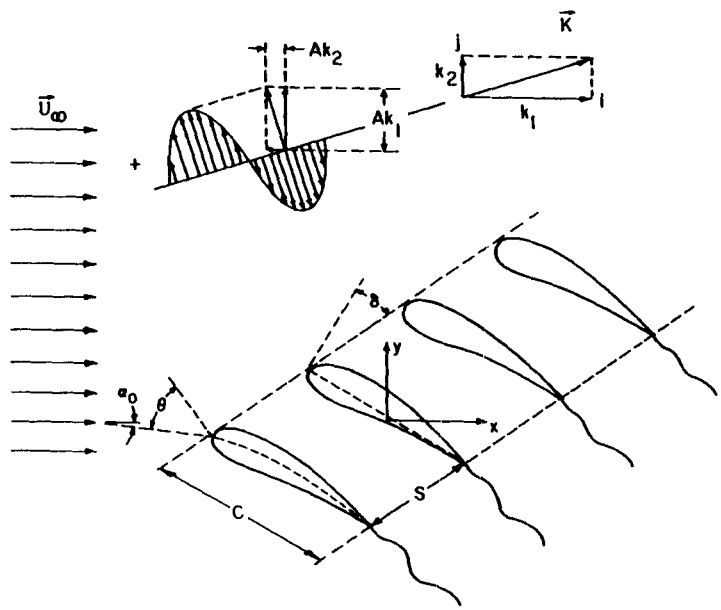

Figure. 1. Flow field schematic

the aerofoils along the stagger line and θ the inlet blade angle. The gust amplitude and harmonic frequency are denoted by A and ω respectively. The two-dimensional gust propagates in the direction $\mathbf{K} = k_1\mathbf{i} + k_2\mathbf{j}$, where k_1 is the reduced frequency and k_2 is the transverse gust wave number, i.e. the transverse component of the gust propagation direction vector.

The complete flow field $\mathbf{Q}(x, y, t)$ is assumed to be comprised of a steady mean flow $\mathbf{Q}_0(x, y)$ and a harmonic gust unsteady flow field $\mathbf{Q}'_G$:

$$\mathbf{Q}(x, y, t) = \mathbf{Q}_0(x, y) + \mathbf{Q}'_G(x, y)\exp(ik_1 t). \tag{1}$$

Steady flow

For the steady flow of an incompressible, inviscid, fluid, a velocity potential function can be defined. The complete flow field is then described by the following Laplace equation:

$$\nabla^2\Phi_0(x, y) = 0, \tag{2}$$

where

$$\mathbf{Q}_0(x, y) = \nabla\Phi_0(x, y).$$

Since the Laplace equation is linear, the velocity potential can be decomposed into components by the superposition principle. In particular, the steady potential is decomposed into non-circulatory components $\Phi_{NC}(x, y)$ and $\Phi_C(x, y)$:

$$\Phi_0(x, y, t) = \Phi_{NC}(x, y) + \Gamma\Phi_C(x, y), \tag{3}$$

where $\nabla^2\Phi_{NC} = 0$, $\nabla^2\Phi_C = 0$ and Γ is the unknown steady flow circulation constant.

To complete the steady flow mathematical model, far-field inlet, far-field exit, aerofoil surface, wake-dividing streamline and cascade periodic boundary conditions must be specified.

The steady far-field inlet flow is uniform (equation (4)), with the mass flow rate specified by the far-field exit boundary conditions (equation (5)):

$$\Phi_{NC}|_{\text{far-field inlet}} = U_\infty x, \tag{4a}$$

$$\Phi_C|_{\text{far-field inlet}} = 0, \tag{4b}$$

$$\left.\frac{\partial\Phi_{NC}}{\partial n}\right|_{\text{far-field exit}} = U_\infty\cos(\alpha_0 + \theta), \tag{5a}$$

$$\left.\frac{\partial\Phi_C}{\partial n}\right|_{\text{far-field exit}} = 0, \tag{5b}$$

where n is the surface unit normal.

A zero normal flow velocity is required on the aerofoil surfaces:

$$\left.\frac{\partial\Phi_{NC}}{\partial n}\right|_{\text{aerofoil}} = 0, \tag{6a}$$

$$\left.\frac{\partial\Phi_C}{\partial n}\right|_{\text{aerofoil}} = 0. \tag{6b}$$

The steady velocity potential is discontinuous along the aerofoil wake-dividing streamline. The steady flow discontinuity is satisfied with a continuous non-circulatory velocity potential and a discontinuous circulatory velocity potential. The steady circulatory potential discontinuity is equal to the steady circulation Γ; also specified is the continuity of the steady non-circulatory

velocity potential along the wake streamline:

$$\Delta\Phi_C|_{wake} = \Phi_C^+ - \Phi_C^- = \Gamma = \Delta\Phi_C|_{TE}, \tag{7a}$$

$$\Delta\Phi_{NC}|_{wake} = 0, \tag{7b}$$

where TE denotes the aerofoil trailing edge and the superscripts + and − denote the upper and lower aerofoil surfaces respectively.

In addition, the Kutta condition is applied, thereby enabling the steady circulation constant Γ to be determined. The Kutta condition is satisfied by requiring the chordwise velocity components on the upper and lower aerofoil surfaces to be equal in magnitude at the trailing edge:

$$|U_0|_{TE}^+ = |U_0|_{TE}^-. \tag{8}$$

The cascade periodic steady velocity potential boundary conditions are given by

$$\Phi_{NC}|_{\text{upper boundary}} = \Phi_{NC}|_{\text{lower boundary}} + U_\infty S \sin(\alpha_0 + \theta) \tag{9a}$$

$$\left.\frac{\partial\Phi_{NC}}{\partial n}\right|_{\text{upper boundary}} = -\left.\frac{\partial\Phi_{NC}}{\partial n}\right|_{\text{lower boundary}}, \tag{9b}$$

$$\Phi_C|_{\text{upper boundary}} = \Phi_C|_{\text{lower boundary}}, \tag{9c}$$

$$\left.\frac{\partial\Phi_C}{\partial n}\right|_{\text{upper boundary}} = -\left.\frac{\partial\Phi_C}{\partial n}\right|_{\text{lower boundary}} \tag{9d}$$

Gust unsteady aerodynamics

The two-dimensional gust unsteady flow field $\mathbf{Q}'_G$ is determined by decomposing the gust-generated unsteady flow field into harmonic rotational, $\mathbf{Q}_R$, and potential, $\mathbf{Q}_P$, components:

$$\mathbf{Q}'_G = \mathbf{Q}_R + \mathbf{Q}_P. \tag{10}$$

The rotational gust component is described by the following linearized unsteady Euler equations, determined by linearizing the unsteady flow about the steady flow field:

$$\nabla\cdot\mathbf{Q}_R = 0, \tag{11a}$$

$$\frac{D_0}{Dt}\mathbf{Q}_R + \mathbf{Q}_R\cdot\nabla(\nabla\Phi_0) = -\frac{1}{\rho}\nabla P_R, \tag{11b}$$

where

$$\frac{D_0}{Dt}(\ ) = \frac{\partial}{\partial t}(\ ) + \mathbf{Q}_0\cdot\nabla(\ )$$

and P_R is the unsteady pressure associated with the rotational gust flow field.

The gust is assumed to be convected with the steady mean flow past the aerofoil cascade and therefore does not interact with the cascade. Thus the following solution for the rotational gust is determined by solving the linearized Euler equations in the far upstream where the steady flow field is uniform:

$$\mathbf{Q}_R = u^+\mathbf{i} + v^+\mathbf{j}, \tag{12}$$

where

$$u^+ = -Ak_2\exp[ik_1(t-x) - ik_2y] \quad \text{and} \quad v^+ = Ak_1\exp[ik_1(t-x) - ik_2y].$$

It should be noted that in this gust solution, the components u^+ and v^+ are coupled, the ratio of their amplitudes being $u^+/v^+ = -k_2/k_1$. Also, this solution corresponds exactly to the Sears

transverse gust[1] when $k_2 = 0$, i.e. $u^+ = 0$ and $v^+ = Ak_1 \exp[ik_1(t-x)]$. However, this gust solution differs from that used in the Horlock[3] and Naumann and Yeh[4] models in which: (1) the two gust components are uncoupled, $u^+ = \vec{u}^+ \exp[ik_1(t-x)]$ and $v^+ = \vec{v}^+ \exp[ik_1(t-x)]$, where $\vec{u}^+$ and $\vec{v}^+$ denote the individual amplitudes of the two gust components, which are independent of each other; (2) the gust and resulting unsteady aerodynamics are independent of the transverse component of the gust propagation direction vector $\mathbf{K} = k_1\mathbf{i} + k_2\mathbf{j}$.

The potential gust component Φ'_G is described by a Laplace equation. The solution is determined by decomposing this potential gust component into circulatory and non-circulatory components $\Phi'_{GC}(x, y)$ and $\Phi'_{GNC}(x, y)$, each of which is individually described by a Laplace equation:

$$\mathbf{Q}_P = \frac{\partial \Phi'_G}{\partial x}\mathbf{i} + \frac{\partial \Phi'_G}{\partial y}\mathbf{j}, \tag{13a}$$

$$\Phi'_G = \Phi'_{GNC} + \Gamma'_G \Phi'_{GC}, \tag{13b}$$

$$\nabla^2 \Phi'_{GC} = 0, \qquad \nabla^2 \Phi'_{GNC} = 0, \tag{13c}$$

where Γ'_G is the unsteady gust circulation.

Boundary conditions must be specified in the far-field inlet, far-field exit, aerofoil surface, wake-dividing streamline and cascade periodic boundary for the gust circlatory and non-circulatory components.

The inlet far-field gust velocity potential boundary conditions are obtained by using a Fourier series to satisfy the periodicity condition at the far upstream:[7]

$$\Phi'_{GNC}|_{\text{far-field inlet}} = -\left|\frac{S}{\beta_0}\right| \left|\frac{\partial \Phi'_{GNC}}{\partial n}\right|_{\text{far-field inlet}}, \tag{14a}$$

$$\Phi'_{GC}|_{\text{far-field inlet}} = -\left|\frac{S}{\beta_0}\right| \left|\frac{\partial \Phi'_{GC}}{\partial n}\right|_{\text{far-field inlet}}, \tag{14b}$$

where β_0 is the interblade phase angle and n is the surface unit normal.

The exit far-field gust non-circulatory potential boundary condition (equation (15a)) is obtained in a manner analogous to that for the inlet. Since the wake does not attenuate in the far-field, the gust circulatory potential boundary condition (equation (15b)) is obtained by solving the Laplace equation at the far-field exit and satisfying the blade-to-blade periodicity condition:[7]

$$\Phi'_{GNC}|_{\text{far-field exit}} = -\left|\frac{S}{\beta_0}\right| \left|\frac{\partial \Phi'_{GNC}}{\partial n}\right|_{\text{far-field exit}}, \tag{15a}$$

$$\Phi'_{GC}|_{\text{far-field exit}} = -e^{-ik_1 x}\left(\frac{e^{k_1 y}}{1 - e^{(k_1 - i\nu)S\cos\delta}} + \frac{e^{-k_1 y}}{1 - e^{-(k_1 + i\nu)S\cos\delta}}\right), \tag{15b}$$

where

$$\nu = \frac{\beta_0 + k_1 \sin\delta/S}{S\cos\delta}.$$

The aerofoil surface boundary conditions specify that the normal velocity of the flow field must be equal to that of the aerofoil:

$$\left.\frac{\partial \Phi'_{GC}}{\partial n}\right|_{\text{aerofoil}} = 0, \tag{16a}$$

$$\left.\frac{\partial \Phi'_{GNC}}{\partial n}\right|_{\text{aerofoil}} = W'_G(x, y) = \text{upwash}. \tag{16b}$$

The gust-generated unsteady rotational and potential flow fields are coupled through the boundary conditions on the non-circulatory gust component. In particular, the aerofoil cascade is stationary, with the rotational gust defined in equation (12) convected with the mean steady flow field. Thus the upwash on the aerofoil, $W'_G(x, y)$, is determined by requiring the normal component of the unsteady flow field to be zero on the aerofoil:

$$\left.\frac{\partial \Phi'_{GNC}}{\partial n}\right|_{\text{aerofoil}} = W'_G(x, y) = -\mathbf{n}\cdot\mathbf{Q}_R$$

or

$$W'_G(x, y) = -A\left(\frac{\partial f}{\partial x}k_2 + k_1\right)\exp[-i(k_1 x + k_2 y)], \tag{17}$$

where $f(x)$ specifies the aerofoil profile.

The gust unsteady velocity potential is discontinuous along the aerofoil wake-dividing streamline. This discontinuity is satisfied with a continuous non-circulatory velocity potential and a discontinuous circulatory velocity potential. The unsteady circulatory velocity potential discontinuity is specified by requiring the pressure to be continuous across the wake and then utilizing the unsteady Bernoulli equation to relate the unsteady velocity potential and the pressure. The resulting circulatory potential wake streamline discontinuity is given in equation (18); also specified is the continuity of the non-circulatory velocity potential along the wake streamline:

$$\Delta\Phi'_{GC}|_{\text{wake}} = \Gamma'_G \exp[-ik(x-1)], \tag{18a}$$

$$\Delta\Phi'_{GNC}|_{\text{wake}} = 0. \tag{18b}$$

The Kutta condition is also applied to the unsteady gust flow field. This enables the unsteady circulation constant Γ'_G to be determined. The Kutta condition is satisfied by requiring no unsteady pressure difference across the aerofoil chordline at the trailing edge. The corresponding relation for the trailing edge gust velocity potential difference is determined from the unsteady Bernoulli equation:

$$\Delta P'_P|_{TE} = P'_P|^{+}_{TE} - P'_P|^{-}_{TE} = 0, \tag{19a}$$

$$(\nabla\Phi_0\cdot\nabla\Phi'_G + ik\Phi'_G)|^{+}_{TE} = (\nabla\Phi_0\cdot\nabla\Phi'_G + ik\Phi'_G)|^{-}_{TE}, \tag{19b}$$

where TE denotes the aerofoil trailing edge, the superscripts + and − denote the upper and lower aerofoil surfaces respectively and P_P is the unsteady pressure associated with the gust potential flow field.

The cascade periodic gust potential boundary conditions are given by

$$\Phi'_{GNC}|_{\text{upper boundary}} = e^{i\beta_0}\Phi'_{GNC}|_{\text{lower boundary}}, \tag{20a}$$

$$\left.\frac{\partial \Phi'_{GNC}}{\partial s}\right|_{\text{upper boundary}} = e^{i\beta_0}\left.\frac{\partial \Phi'_{GNC}}{\partial s}\right|_{\text{lower boundary}}, \tag{20b}$$

$$\Phi'_{GC}|_{\text{upper boundary}} = e^{i\beta_0}\Phi'_{GC}|_{\text{lower boundary}}, \tag{20c}$$

$$\left.\frac{\partial \Phi'_{GC}}{\partial s}\right|_{\text{upper boundary}} = e^{i\beta_0}\left.\frac{\partial \Phi'_{GC}}{\partial s}\right|_{\text{lower boundary}}, \tag{20d}$$

where s is the unit vector along the stagger line of the cascade.

The unsteady dependent variable of primary interest is the unsteady pressure P'_G, from which the unsteady aerodynamic lift on the aerofoil is calculated. It is determined from the solution for the steady and unsteady gust velocity potentials, the unsteady Bernoulli equation and the unsteady rotational gust pressure P_R:

$$P'_G = P_P + P_R = -\nabla\Phi_0 \cdot \nabla\Phi'_G - ik_1\Phi'_G + P_R. \tag{21}$$

COMPUTATIONAL DOMAIN

Computational grid

A boundary-fitted computational grid generation technique is utilized for the numerical solution.[8] A Poisson-type grid solver is used to fit a C-type grid around a reference aerofoil in the cascade. This method permits grid points to be specified along the entire boundary of the computational plane. As depicted in Figure 2, the boundary in the physical plane is denoted by the curve a–b–c–d–e–f–g–h–i–a and encompasses the aerofoil, its wake, the far-field inlet, the far-field exit and the cascade periodic boundaries. The application of this grid generation technique results in an equally spaced, orthogonal computational grid at the interior points in the transformed (ξ, η) plane. Attractive features of this technique include: mesh clustering in regions of high surface curvature; high grid orthogonality, especially in the near-aerofoil surface and periodic boundary regions; and the establishment of periodic grids for ease of enforcing cascade

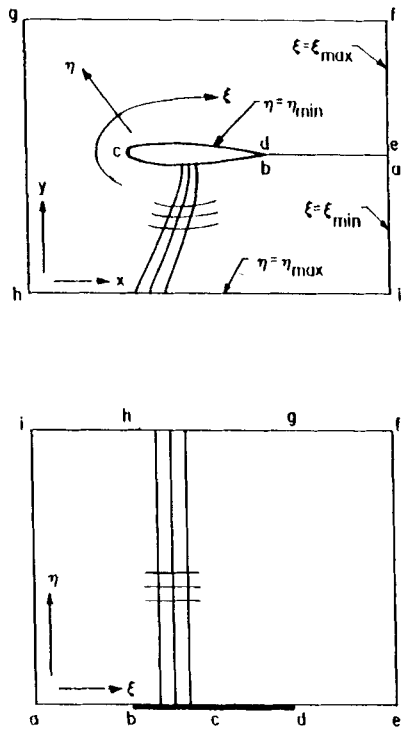

Figure. 2. Body-fitted co-ordinate transformation

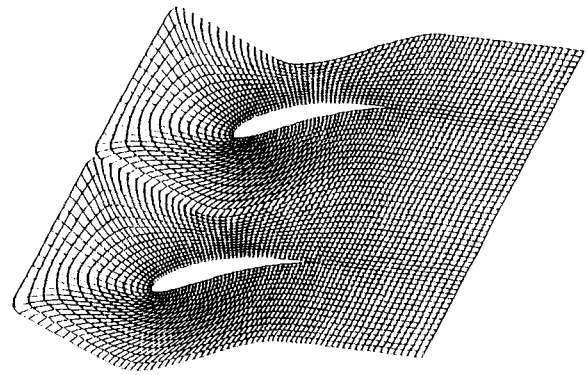

Figure. 3. Gostelow cascade computational grid

periodic boundary conditions. A typical boundary-fitted grid for a Gostelow aerofoil cascade is shown in Figure 3.

Laplace equations describe the complete flow field including the unknown velocity potentials Φ_{NC}, Φ_C, Φ'_{GNC} and Φ'_{GC} (equations (3) and (13)). In the transformed (ξ, η) co-ordinate system the Laplace equation takes on the following non-homogeneous form:

$$\frac{\partial^2\bar{\Phi}}{\partial\xi^2} + \alpha\frac{\partial^2\bar{\Phi}}{\partial\eta^2} - 2\alpha\beta\frac{\partial\bar{\Phi}}{\partial\eta} - 2\gamma\frac{\partial\bar{\Phi}}{2\xi} = F(\xi, \eta), \tag{22}$$

where $\bar{\Phi}$ is a shorthand method of writing these four velocity potentials in the transformed plane, i.e. $\bar{\Phi}$ denotes $\Phi_{NC}(\xi, \eta)$, $\Phi_C(\xi, \eta)$, $\Phi'_{GNC}(\xi, \eta)$ or $\Phi'_{GC}(\xi, \eta)$; $F(\xi, \eta)$ contains the cross-derivative term $\partial^2\bar{\Phi}/\partial\xi\,\partial\eta$, and the coefficients α, β and γ are functions of the transformed co-ordinates ξ and η which are treated as constants in each individual grid element.

Analytical solution

To obtain the analytical solution to the transformed Laplace equation, it is first rewritten as a homogeneous equation by defining a new dependent variable $\hat{\phi}(\xi, \eta)$:

$$\frac{\partial^2\hat{\phi}}{\partial\xi^2} + \alpha\frac{\partial^2\hat{\phi}}{\partial\eta^2} - (\gamma^2 + \alpha\beta^2)\hat{\phi} = 0, \tag{23}$$

where

$$\bar{\Phi} = \hat{\phi}\exp(\gamma\xi + \beta\eta) - \frac{F(\gamma\xi + \beta\eta)}{2(\gamma^2 + \alpha\beta^2)}.$$

The general solution for $\hat{\phi}$ is determined by separation of variables and is given by

$$\hat{\phi}(\xi, \eta) = [A_1\cos(\lambda\xi) + A_2\sin(\lambda\xi)][B_1\cos(\mu\eta) + B_2\sin(\mu\eta)], \tag{24}$$

where $\mu = [(\gamma^2 + \alpha\beta^2 + \lambda^2)/\alpha]^{1/2}$ and λ, A_1, A_2, B_1 and B_2 are constants to be determined from the boundary conditions.

LOCALLY ANALYTICAL SOLUTION

Analytical solutions in individual computational grid elements are determined by applying proper boundary conditions on each element to evaluate the unknown constants in the general

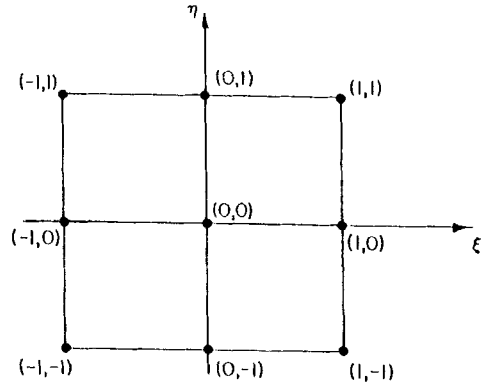

Figure. 4. Computational grid element

velocity potential solution specified in equation (24). The solution to the global problem is then determined through the application of the global boundary conditions and the assembly of the locally analytical solutions.

A typical computational grid element is schematically depicted in Figure 4. The local element boundary conditions specify the values of the various velocity potentials at the eight boundary nodal points. However, to obtain unique analytical solutions to the Laplace equation in this element, i.e. to determine the values of the integration constants in the general solution for each element, continuous boundary conditions are required on all four boundaries. For numerical purposes, these boundary conditions are expressed in an implicit formulation in terms of the three known nodal values on each element boundary. In particular, a combination of a linear and an exponential function is utilized on each boundary as they satisfy the Laplace equation:

$$\hat{\phi}(\xi, 1) = a_1^{(1)}\exp(\xi) + a_2^{(1)}\xi + a_3^{(1)}, \tag{25a}$$

$$\hat{\phi}(1, \eta) = a_1^{(2)}\exp(\eta) + a_2^{(2)}\eta + a_3^{(2)}, \tag{25b}$$

$$\hat{\phi}(\xi, -1) = a_1^{(3)}\exp(\xi) + a_2^{(3)}\xi + a_3^{(3)}, \tag{25c}$$

$$\hat{\phi}(-1, \eta) = a_1^{(4)}\exp(\eta) + a_2^{(4)}\eta + a_3^{(4)}, \tag{25d}$$

where the constants $a_1^{(i)}$, $a_2^{(i)}$ and $a_3^{(i)}$ are determined from the known values at the three nodal points on each boundary.

The general analytical solution to the Laplace equation given in (24) is valid in individual grid elements as well as over the complete flow region. To determine the relationship between the velocity potential at the centre of the typical grid element (Figure 4) and its surrounding values, the superposition principle is used to decompose $\hat{\phi}$ into four components, each having only one non-homogeneous boundary condition:

$$\begin{aligned}\hat{\phi}(\xi, \eta) = \sum_{n=1}^{\infty} \{ & A_{n1}\sinh[\mu_n(\eta + 1)]\sin[\lambda_n(\xi + 1)] \\ & + A_{n2}\sinh[\mu_n(\eta - 1)]\sin[\lambda_n(\xi + 1)] \\ & + A_{n3}\sinh[\mu_n'(\xi + 1)]\sin[\lambda_n(\eta + 1)] \\ & + A_{n4}\sinh[\mu_n'(\xi - 1)]\sin[\lambda_n(\eta + 1)]\},\end{aligned} \tag{26}$$

where $\lambda_n = n\pi/2$, $\mu_n = [(\gamma^2 + \beta^2\alpha + \lambda_n^2)/\alpha]^{1/2}$ and $\mu_n' = (\gamma^2 + \beta^2\alpha + \lambda_n^2\alpha)^{1/2}$.

Application of the local boundary conditions (equation (25)) together with the orthogonality of the Fourier series lead to the following values for A_{ni}:

$$A_{ni} = C_{1ni}\hat{\phi}(1, 1) + C_{2ni}\hat{\phi}(1, 0) + C_{3ni}\hat{\phi}(1, -1) + C_{4ni}\hat{\phi}(0, -1) + C_{5ni}\hat{\phi}(-1, -1) + C_{6ni}\hat{\phi}(-1, 0) + C_{7ni}\hat{\phi}(-1, 1) + C_{8ni}\hat{\phi}(0, 1), \tag{27}$$

where the constants $C_{1ni}, \ldots, C_{8ni}$ are functions of the $a_1^{(i)}$ $a_2^{(i)}$ and $a_3^{(i)}$ boundary constants.

With the analytical solution in an individual grid element thus specified (equations (26) and (27)), the value of $\hat{\phi}$ at the centre of the element can be written as follows:

$$\hat{\phi}(0, 0) = \sum_{n=1}^{\infty} \{[(A_{n1} - A_{n2})\sinh(\mu_n) + (A_{n3} - A_{n4})\sinh(\mu_n')]\sin(\lambda_n)\}. \tag{28}$$

Substituting for the A_{ni} terms (equation (27)) leads to the following:

$$\hat{\phi}(0, 0) = C_1'\hat{\phi}(1, 1) + C_2'\Phi(1, 0) + C_3'\hat{\phi}(1, -1) + C_4'\hat{\phi}(0, -1) - C_5'\hat{\phi}(-1, -1) + C_6'\hat{\phi}(-1, 0) + C_7'\hat{\phi}(-1, 1) + C_8'\hat{\phi}(0, 1), \tag{29}$$

where the constants $C_1', C_2', \ldots, C_8'$ are functions of the $a_1^{(i)}$, $a_2^{(i)}$ and $a_3^{(i)}$ boundary constants as well as the transformed co-ordinate functions α, β and γ.

This solution for $\hat{\phi}$ at the centre point is rewritten in term of the original dependent variable $\bar{\Phi}$ as follows:

$$\bar{\Phi}(0, 0) = C_1\bar{\Phi}(1, 1) + C_2\bar{\Phi}(1, 0) + C_3\bar{\Phi}(1, -1) + C_4\bar{\Phi}(0, -1) + C_5\bar{\Phi}(-1, -1) + C_6\bar{\Phi}(-1, 0) + C_7\bar{\Phi}(-1, 1) + C_8\bar{\Phi}(0, 1), \tag{30}$$

where the constants $C_1, C_2, \ldots, C_8$ are again functions of the $a_1^{(i)}$, $a_2^{(i)}$ and $a_3^{(i)}$ boundary constants as well as the transformed co-ordinate functions α, β and γ.

Thus the local analytical algebraic equation relating the value of the velocity potential at the centre of the computational element to its neighbouring eight known nodal values has been completely determined.

Computational procedure

The above technique is applied to adjacent grid elements, with the boundary nodal point considered as the interior point. For a general grid element with centre at (i, j), the resulting algebraic relation between the centre value of the velocity potential and its eight surrounding nodal values is given by

$$\bar{\Phi}(i, j) = C_{i+1, j+1}\bar{\Phi}(i + 1, j + 1) + C_{i+1, j}\bar{\Phi}(i + 1, j) + C_{i+1, j-1}\bar{\Phi}(i + 1, j - 1) + C_{i, j-1}\bar{\Phi}(i, j - 1) + C_{i-1, j-1}\bar{\Phi}(i - 1, j - 1) + C_{i-1, j}\bar{\Phi}(i - 1, j) + C_{i-1, j+1}\bar{\Phi}(i - 1, j + 1) + C_{i, j+1}\bar{\Phi}(i, j + 1), \tag{31}$$

where $2 \leqslant i \leqslant i_{\max} - 1$, $2 \leqslant j \leqslant j_{\max} - 1$ and the C_{ij} are functions of the $a_1^{(i)}$, $a_2^{(i)}$ and $a_3^{(i)}$ boundary constants as well as the transformed co-ordinate functions α, β and γ.

The global boundary conditions are specified by

$$\bar{\Phi}(i, 1) = \text{aerofoil and wake boundary conditions}, \quad 1 \leqslant i \leqslant i_{\max}, \tag{32a}$$

$$\bar{\Phi}(i, j_{\max}) = \text{far-field inlet and cascade periodic boundary conditions}, \quad 1 \leqslant i \leqslant i_{\max}, \tag{32b}$$

$$\bar{\Phi}(i_{\max}, j) = \text{far-field exit boundary conditions}, \quad 1 < j < j_{\max}, \tag{32c}$$

$$\bar{\Phi}(1, j) = \text{far-field exit boundary conditions}, \quad 1 < j < j_{\max}. \tag{32d}$$

These global boundary conditions together with the interior point solution specified in equation (31) for $\bar{\Phi}(i, j)$, where $2 \leqslant i \leqslant i_{\max} - 1$ and $2 \leqslant j \leqslant j_{\max} - 1$, lead to a system of algebraic equations. For a fixed j-value:

$$\begin{aligned} -C_{i-1,j}\bar{\Phi}(i-1,j) + \bar{\Phi}(i,j) - C_{i+1,j}\bar{\Phi}(i+1,j) &= C_{i+1,j+1}\bar{\Phi}(i+1,j+1) \\ + C_{i-1,j+1}\bar{\Phi}(i-1,j+1) + C_{i,j+1}\bar{\Phi}(i,j+1) &+ C_{i+1,j-1}\bar{\Phi}(i+1,j-1) \\ + C_{i-1,j-1}\bar{\Phi}(i-1,j-1) + C_{i,j-1}\bar{\Phi}(i,j-1). & \end{aligned} \tag{33}$$

The right-hand side of this equation is comprised of known quantities, i.e. the $(j-1)$-terms are known from the boundary conditions ($j = 2$) or the last sweep, with the $(j+1)$-terms determined from the boundary condition ($j = j_{\max} - 1$) or the previous iteration.

Equation (33) can be written as a tridiagonal matrix, with the matrix solved by Thomas algorithm for all j-values ($2 \leq j \leq j_{\max} - 1$). This procedure is then iterated by successive over-relaxation until the entire solution converges.

RESULTS

Model and solution verification

The strong dependence of the gust-generated unsteady aerodynamics on the steady effects of aerofoil and cascade geometry and incidence angle are manifested in the coupling of the unsteady and steady flow fields through the unsteady boundary conditions. Hence valid gust response predictions require an accurate analysis of the steady flow field. It is thus necessary to verify both the steady and the unsteady modelling and locally analytical solutions.

The ability of the steady flow model and locally analytical solution to accurately predict cascade flow fields is demonstrated by analysing the theoretical cascade initially considered by Gostelow.[9] This cascade, shown in Figure 3, is characterized by a stagger angle of 37·5°, a solidity of 1·01, with aerofoils having an 11·25% thickness-to-chord ratio and 32° of camber. The correlation of the predicted chordwise distribution of the aerofoil surface static pressure coefficient $\bar{C}_p$ obtained with the model and solution developed herein and that of Gostelow is presented in Figure 5. There is excellent correlation between the two analyses.

To verify the unsteady aerodynamic gust mathematical model and locally analytical solution, predictions are correlated with those from the classical Whitehead analysis.[2] A flat plate aerofoil cascade with a solidity of 1·01 and a stagger angle of 37·5° is considered, with the computational grid shown in Figure 6. The complex aerofoil surface unsteady pressure differences generated by a convected transverse gust with a reduced frequency of 0·8 for a wide range of interblade phase angles are presented in Figure 7. The excellent correlation between the predictions from the two models is readily apparent.

Experiment correlation

An experimental investigation of the gust-generated unsteady aerodynamic response of a vane row in an extensively instrumented axial flow research compressor at realistically high values of the reduced frequency is described in Reference 10. The aerodynamic forcing function to the vane row generated by the upstream aerofoil wakes and the resulting downstream vane surface

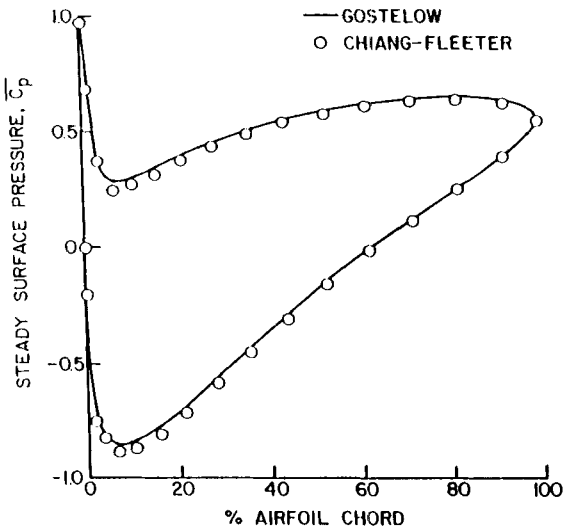

Figure. 5. Gostelow cascade static pressure correlation

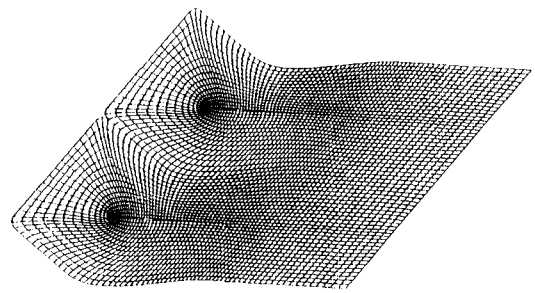

Figure. 6. Flat plate cascade computational grid

chordwise unsteady pressure distributions were measured. These data were Fourier-decomposed, with the final data quantifying both the chordwise and transverse gust components of the forcing function, the chordwise distribution of the unsteady pressure difference coefficient, and the steady vane surface static pressure distributions.

Predictions from the model and locally analytical solution developed herein are correlated with data for both low and high steady loading operating conditions, characterized by incidence angles of 1·0° and 5·5° degrees respectively. The vane profile and row geometry are depicted in Figure 8 which presents the computational grid. The predicted chordwise distribution of the vane surface static pressure exhibits excellent correlation with the data for both steady loading conditions (Figures 9 and 10). The data–theory correlations of the unsteady pressure differences across the vane chordine at 1·0° and 5·5° incidence are presented in Figures 11 and 12. Also presented as a reference are the corresponding classical flat plate cascade predictions of Whitehead.[2] The

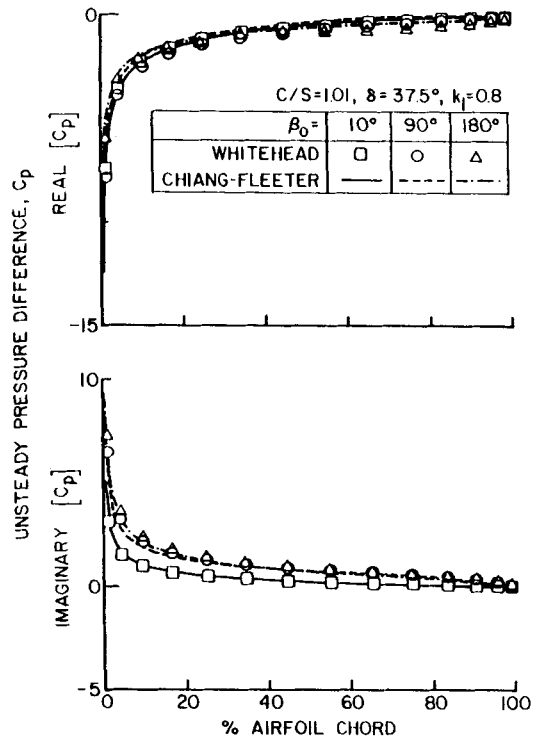

Figure. 7. Flat plate cascade unsteady pressure correlation

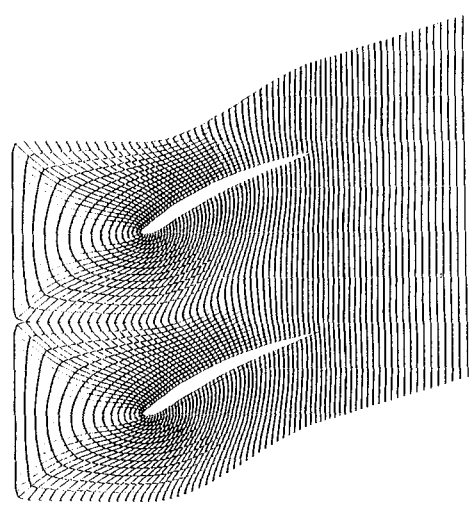

Figure. 8. Compressor vane geometry and computational grid

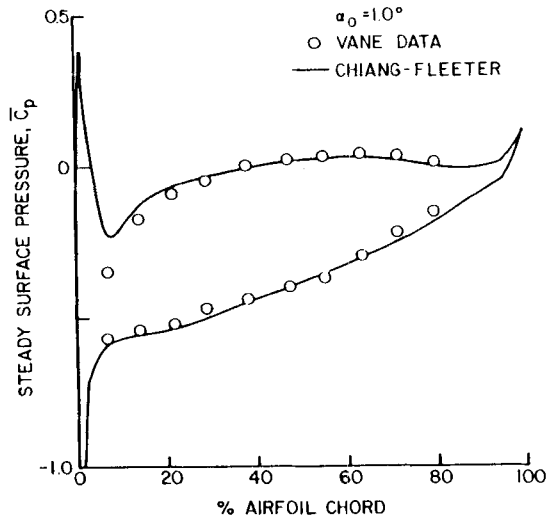

Figure. 9. Vane static pressure correlation at low steady loading

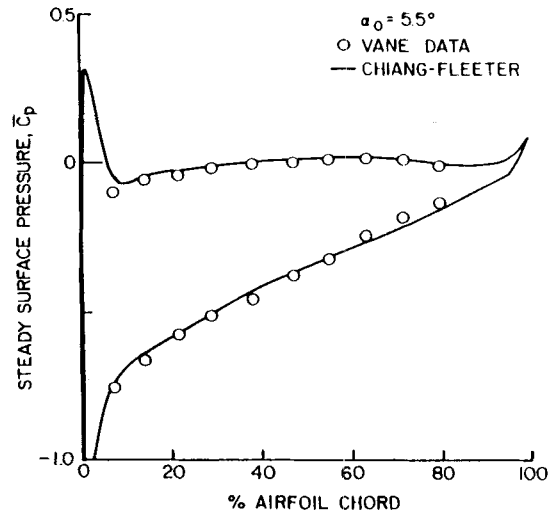

Figure. 10. Vane static pressure correlation at high steady loading

correlation between the predictions and the data are similar for the two steady loading conditions considered. Both predictions exhibit relatively good correlation with the unsteady pressure difference magnitude data, with the chordwise variation of the Chiang–Fleeter cambered aerofoil predictions analogous to that of the data. The phase data are in very good agreement with the predictions from the model developed herein, with relatively poor agreement between the data and the flat plate predictions. This is a result of the coupling between the unsteady and steady flow fields.

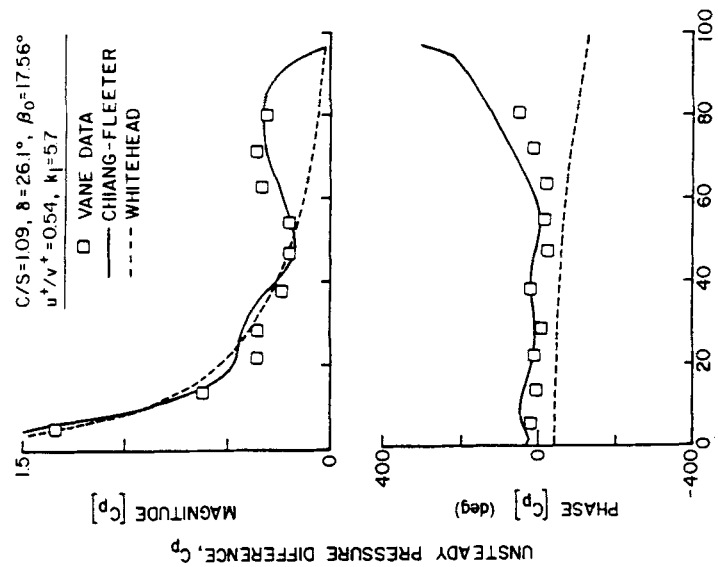

Figure. 12. Vane unsteady pressure correlation at high steady loading

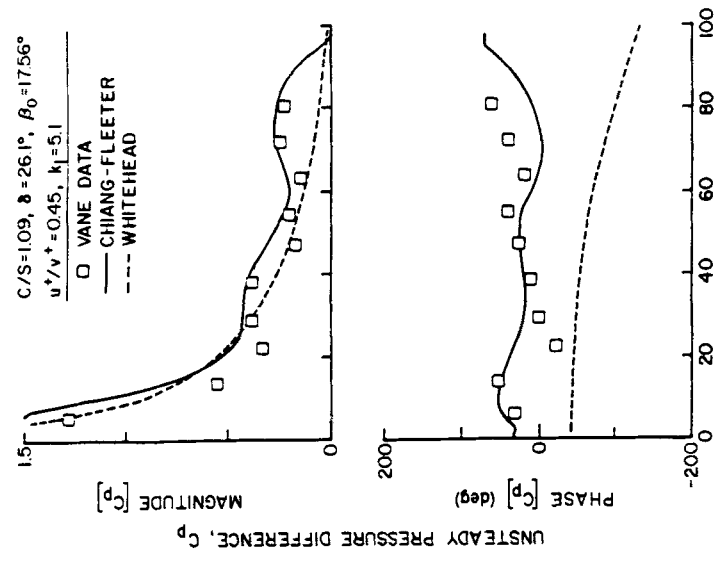

Figure. 11. Vane unsteady pressure correlation at low steady loading

Steady loading effects

This model and locally analytical solution are utilized to demonstrate the effects of steady loading on the gust response of a cambered aerofoil cascade. This is accomplished by analysing the gust-generated unsteady aerodynamics on the Gostelow cascade geometry over a range of steady loading conditions, characterized by the incidence angle value. In particular, the Gostelow cascade steady flow field and unsteady aerodynamics due to two-dimensional gust at an angle of 26·6° and a unity reduced frequency are analysed for mean flow incidence angles of 0°, 10° and 20°.

The predicted chordwise distributions of the aerofoil surface static pressure coefficients $\bar{C}_p$ for mean flow incidence angles of 0°, 10° and 20° are presented in Figure 13. Increasing the incidence angle has a large effect on the steady loading distribution, particularly on the front part of the aerofoil. Forward of approximately 20% chord, the steady surface pressure decreases on the suction surface and increases on the pressure surface. Aft of this chord location, the pressure increases on both surfaces of the aerofoil.

The effect of increasing the mean flow incidence angle on the gust-generated complex unsteady pressure difference across the chordline of the aerofoil, C_p, is shown in Figure 14. Both the magnitude and the phase lag of the unsteady pressure difference are dependent on the incidence angle, with the largest effects found over the front portion of the aerofoil, analogous to the steady results. This is a result of the strong dependence of the unsteady aerodynamics on the steady effects of aerofoil and cascade geometry and mean flow incidence angle, modelled by the coupling of the unsteady and steady flow fields through the unsteady boundary conditions. As a reference, the corresponding prediction from the classical transverse gust Whitehead zero-incidence flat plate aerofoil cascade model is also shown. The very large differences between the predictions from these two models are readily apparent. These are due to the coupling of the steady and unsteady flow fields for thick, cambered aerofoils at finite mean flow incidence angles as well as the coupled transverse and chordwise gust, which are included in the flow model developed herein but not in the Whitehead model.

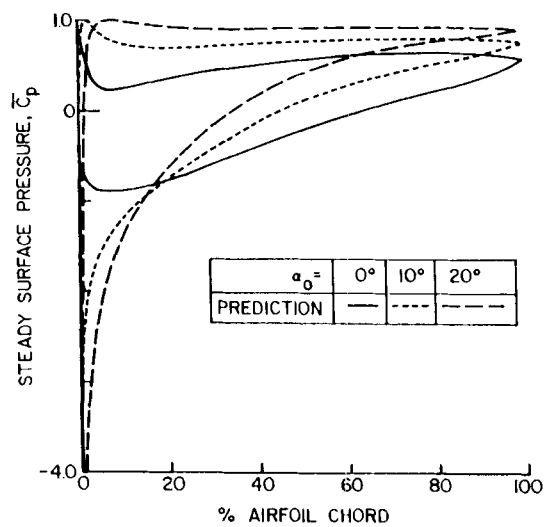

Figure. 13. Effect of incidence angle on Gostelow cascade static pressure

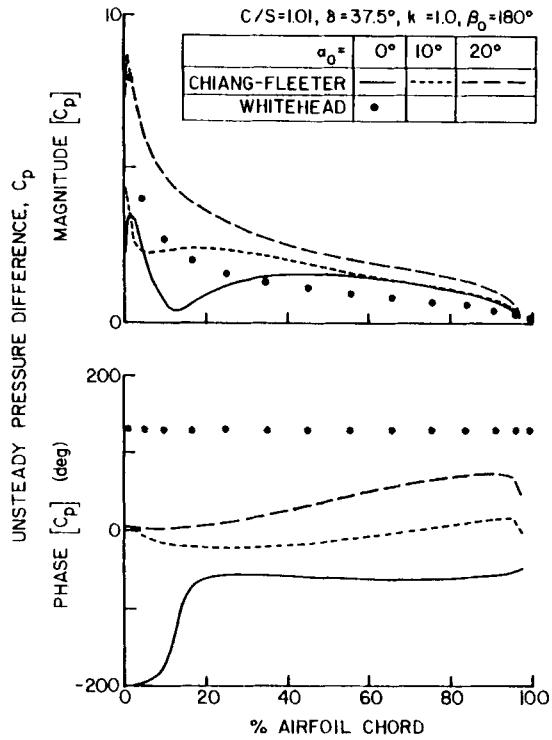

Figure. 14. Effect of incidence angle on Gostelow cascade unsteady pressure

CONCLUSIONS

The unsteady aerodynamic response of a cascade comprised of arbitrary thick and cambered aerofoils in an incompressible, inviscid, flow field to a convected gust was analysed by developing a complete first-order model. The flow was analysed by considering a periodic flow channel with the velocity potential separated into steady and unsteady harmonic components. The unsteady flow field was considered to be rotational and was linearized about the full steady potential flow past the cascade to account for the effects of aerofoil profile and mean flow incidence. The steady potential flow field and the potential component of the unsteady flow were individually described by Laplace equations, with the unsteady potential decomposed into circulatory and non-circulatory parts.

A locally analytical solution was developed. In this technique the discrete algebraic equations which represent the flow field equations are obtained from analytical solutions in individual grid elements. A body-fitted computational grid is utilized. General analytical solutions to the transformed Laplace equations were developed by applying these solutions to individual grid elements. The complete flow field was then determined by assembling these locally analytical solutions.

The validities of this model and solution technique were demonstrated by correlating predictions with theoretical results for the Gostelow cascade and a classical flat plate aerofoil cascade respectively. This model was then applied to the vane row of an axial flow research compressor. Excellent data–prediction correlation was obtained for the steady and the gust-generated unsteady vane surface pressure distributions at both low and high steady loading conditions.

Finally, the strong dependence of the unsteady aerodynamics on the steady flow field was demonstrated by predicting the effects of steady aerodynamic loading on the gust response of the Gostelow cascade.

ACKNOWLEDGEMENTS

Support of this research program, in part, by the Air Force Office of Scientific Research and NASA Lewis is most gratefully acknowledged.

APPENDIX: NOMENCLATURE

b	aerofoil semichord, $C/2$
$\bar{C}_p$	steady surface static pressure, $p/\frac{1}{2}\rho U_\infty^2$
C_p	unsteady pressure difference, $\Delta p/\rho U_\infty \lvert v^+ \rvert$
α_0	mean incidence angle
$\mathbf{U}_\infty$	far-field uniform mean flow
A	gust amplitude
ω	gust harmonic frequency
$\mathbf{K}$	gust propagation direction vector
k_1	reduced frequency, $\omega b/U_\infty$
k_2	transverse gust wave number
$\mathbf{Q}$	complete flow field
$\mathbf{Q}_o$	steady mean flow
$\mathbf{Q}'_G$	gust-generated unsteady flow
Φ_o	steady velocity potential
Γ	steady circulation constant
Γ'	unsteady circulation constant
β_o	interblade phase angle
θ	inlet blade angle
$\mathbf{Q}_R$	rotational unsteady flow field
$\mathbf{Q}_P$	potential unsteady flow field
P_R	unsteady pressure associated with rotational flow
u^+	chordwise gust component
v^+	transverse gust component
Φ'_G	unsteady harmonic gust potenntial
Φ'_{GC}	circulatory gust velocity potential
Φ'_{GNC}	non-circulatory gust velocity potential
P_P	unsteady pressure associated with potential flow
P'_G	total unsteady pressure
δ	cascade stagger angle

REFERENCES

1. W. R. Sears, 'Some aspects of non-stationary airfoil theory and its practical application', *J. Aeronaut. Sci.* **8,** 104 (1941).
2. D. S. Whitehead, 'Force and moment coefficients for vibrating airfoils in cascade', *ARC R & M 3254*, February 1960.
3. J. H. Horlock, 'Fluctuating lift forces on airfoils moving through transverse and chordwise gusts', *ASME J. Bas. Eng.*, **90,** 494–500 (1968).
4. H. Naumann and H. Yeh, 'Lift and pressure fluctuations of a cambered airfoil under periodic gusts and applications to turbomachinery', *ASME Paper 72-GT-30*, 1972.

5. M. E. Goldstein, and H. Atassi, 'A complete second-order theory for the unsteady flow about an airfoil due to a periodic gust', *J. Fluid Mech.*, **74,** 741–754 (1976).
6. H. M. Atassi, 'The Sears problem for a lifting airfoil revisited—new results', *J. Fluid Mech.*, **141,** 109–122 (1984).
7. J. M. Verdon, 'The unsteady flow in the far field of an isolated blade row', *United Technologies Research Center Report R87-95733301*, April 1987.
8. R. M. Moore and J. D. Hoffman, 'Calculation of unsteady three-dimensional inviscid flows through turbine blade rows', private communication, 1987.
9. J. P. Gostelow, *Cascade Aerodynamics*, Pergamon Press, New York, 1984.
10. V. R. Capece and S. Fleeter, 'Unsteady aerodynamic interactions in a multistage compressor', *ASME J. Turbomachinery*, **109,** 420–428 (1987).